

Catalog of Unconventional Magnons in Collinear Magnets

Xiaobing Chen^{2,1}, Yuntian Liu¹, Pengfei Liu¹, Yutong Yu¹, Jun Ren¹, Jiayu Li¹,
Ao Zhang¹ and Qihang Liu^{1,2,3*}

¹Department of Physics and Guangdong Basic Research Center of Excellence for Quantum Science, Southern University of Science and Technology, Shenzhen 518055, China

²Quantum Science Center of Guangdong–Hong Kong–Macao Greater Bay Area (Guangdong), Shenzhen 518045, China

³Guangdong Provincial Key Laboratory of Computational Science and Material Design, Southern University of Science and Technology, Shenzhen 518055, China

*Email: liuqh@sustech.edu.cn

Abstract

Topological magnons have garnered significant interest for their potential in both fundamental research and device applications, owing to their exotic, uncharged, yet topologically protected boundary modes. However, their comprehension has been hindered by the absence of fundamental symmetry descriptions of magnetic materials, which are primarily governed by isotropic Heisenberg interactions in spin Hamiltonians. The ensuing magnon dispersions enable gapless magnon band nodes that go beyond the scenario of representation theory of the magnetic space groups (MSGs), thus referred to as unconventional magnons. Here we developed spin space group (SSG) theory to elucidate collinear magnetic configurations, classifying the 1421 collinear SSGs into four types, constructing their band representations, and providing a comprehensive tabulation of unconventional magnons, such as duodecuple points, octuple nodal lines, and charge-4 octuple points. Based on the MAGNDATA database, we identified 498 collinear magnets with unconventional magnons, among which over 200 magnon band structures were obtained by using first-principles calculations and linear spin wave theory. Additionally, we evaluated the influence of the spin-orbit coupling-induced exchange interaction in these magnets and found that more than 80% are predominantly governed by the Heisenberg interactions, indicating that SSG serves as an ideal framework for describing magnon band nodes in most

3d, 4d and half-filled 4f collinear magnets. Our work offers new pathways for exploring uncharged transports in magnonic systems, holding promise for advancements in next-generation spintronic devices.

Symmetry plays a crucial role in comprehending various phenomena in condensed matter, particularly for the dispersion and topology of diverse quasiparticles. The electronic topological diagnosis has enjoyed recent success in identifying thousands of materials with topological electronic bands¹⁻⁶, and there is increasing interest in extending these principles to bosonic quasiparticles like magnons. Magnonic systems provide a fertile playground for bosonic topology, e.g., Dirac⁷⁻⁹, Weyl¹⁰⁻¹² and triply-degenerate¹³ magnons, leading to plenty of exotic phenomena¹⁴ such as charge-free topologically protected boundary modes^{7,10,15}, magnon thermal Hall effect^{13,16} and magnon spin Nernst effect^{17,18}. Thus, finding magnetic materials that contain such topological magnons is an area of high interest and demand, with potential applications in next-generation ultrafast spintronic devices and quantum computing^{19,20}.

However, extending the success of topological quantum chemistry theory and material diagnosis from electrons to magnons faces a significant challenge in the fundamental symmetry description of magnetic materials. The conventional framework for describing the symmetry of magnetic materials²¹ and designing magnon band nodes²²⁻²⁴ enforced by symmetry is based on magnetic space groups (MSGs). These groups completely lock the rotational operations in spin space and real space. Nevertheless, the magnon dispersions, especially in collinear magnets with small spin-orbital coupling (SOC) effects [e.g., Dzyaloshinskii-Moriya (DM) interaction^{25,26}], predominantly depend on the isotropic Heisenberg exchange interaction²⁷. The corresponding spin Hamiltonian permits more symmetry operations with separated spin and spatial operations than MSGs. As a result, even though the material candidates for experimental measurements are rare, the existing experimentally observed magnon spectra still cannot be entirely explained by MSGs²⁷⁻³⁰. Examples include the observed Dirac and sextuple points in collinear antiferromagnet (AFM) Cu_3TeO_6 ^{9,31}, the two-fold nodal plane in collinear ferromagnet (FM) Gd ^{32,33}, and doubly degenerate magnon modes in collinear AFMs¹⁷.

To address these challenges, enhanced symmetry groups that describe the magnon band nodes beyond the conventional MSGs, termed unconventional magnons, are required. Spin space groups (SSGs), which were first proposed in the 1960s (yet

overlooked until the recent development of AFM spintronics^{29,30,34-54}), provide a framework that allows for decoupling of spatial and spin operations, and an examination of the symmetries associated with magnon dispersions^{27,28,30}. However, the absence of magnonic material databases and fundamental SSG theories has impeded the understanding of emergent quasiparticles and the systematic search for unconventional magnonic systems.

In this work, we develop the SSG theory describing collinear magnetic configurations, which are typically dictated by Heisenberg exchange interaction, and apply it to the comprehensive search of unconventional magnons in real materials. We categorize the 1421 collinear SSGs into four types, corresponding to all the type-I, III, and IV MSGs yet with more spatial-free spin symmetries and thus different band representations. By employing the representation theory, we not only capture the band degeneracies to reconcile the results of previous experiments, but also tabulate all possible unconventional magnons such as duodecuple (12-fold) nodal point, charge-4 octuple (8-fold) point, octuple nodal line, quadruple nodal plane, and altermagnetic-splitting chiral magnon. Thanks to the $SO(2)$ spin symmetry, the nature of unconventional magnons explored here can be straightforwardly applied to electronic structures without considering spin-1/2 double-group representations. We further conduct high-throughput *ab initio* calculations on the magnon band dispersions and representations for 415 computable collinear magnets within MAGNDATA material database⁵⁵, which adopts experimentally confirmed magnetic structures. Based on an efficient and systematic diagnosis, we identify more than 200 unconventional magnonic materials by the calculated bilinear magnetic exchange coefficients and magnon dispersions. By comparing the results with and without SOC, we evaluate the magnitude of anisotropic interactions and thus the validity of unconventional magnons within the SSG scenario. Finally, we provide the full array of data of collinear SSG theory, including general positions, Wyckoff positions, spin Brillouin zones, little co-groups of wavevectors, band representations, and the magnon dispersions of calculated magnets in our homemade online program and database FINDSPINGROUP (findspingroup.com)⁵⁶.

Categories of 1421 collinear spin space groups

Beginning with 90 spin point groups describing collinear magnetic orders²⁹, 1421 SSGs for collinear magnets can be constructed by group extension⁵². A typical SSG

operation is written as $\{O_s||O_r\}$, where O_s and O_r denote the operation in spin space and real space, respectively. In general, SSGs can be expressed as $G_{SS} = G_{NSS} \times G_{SO}$, where G_{SO} stands for the spin-only group that only contains spin operations $\{O_s||E\}$; G_{NSS} stands for the nontrivial spin space group that contains no pure spin operations⁵⁷. For collinear magnetic structures, $G_{SO} = Z_2^K \times SO(2)$, where $SO(2) = \{U_z(\phi), \phi \in [0, 2\pi)\}$ contains full spin rotations along the spin axis z , $Z_2^K = \{E, TU_n(\pi)\}$ contains the product of time-reversal T and a two-fold spin rotation about any axis \mathbf{n} perpendicular to the z -axis²⁹.

For collinear FM materials with only one type of magnetic sublattice, spatial operations cannot couple any spin operations that change the spin direction. Therefore, the nontrivial spin space group is given by $G_{NSS} = \{E||G\}$, where G is the space group (230 in total). These SSGs are also sufficient to describe the symmetry of collinear ferrimagnet (FIM) that contains multiple spin sublattices yet without any symmetry connecting them. For collinear AFM with two sublattices carrying opposite spins, G_{NSS} is obtained by group extension $\{E||G_\uparrow\} + \{U_n(\pi)||AG_\uparrow\}$, where sublattice space group G_\uparrow contains all spatial symmetries that do not exchange atoms from different sublattices; $\{U_n(\pi)||A\}$ is the symmetry operation that simultaneously reverses the spins and exchanges the two sublattices.

In analogy with the construction of type-I, III and IV MSGs, 1421 collinear SSGs are constructed, including 230 type-I SSGs describing collinear FM/FIM and 1191 SSGs describing collinear AFM. Compared with 674 type-III MSGs, we further categorize collinear SSGs using $\{U_n(\pi)||A\}$, including 252 type-II SSGs with $A = P$ (space inversion), and 422 type-III SSGs with $A = C_n, PC_n$ ($n = 2, 4$) (space rotations and rotoinversions). Such classification naturally leads to the separation of conventional PT-symmetric antiferromagnets with two-fold spin degenerate bands (type-II SSGs) and the recently emerged altermagnets with AFM-induced spin splitting (type-III SSGs)^{37,40,41}. Besides, there are 517 type-IV SSGs describing AFMs with $A = \tau$ (fractional lattice translation). All collinear SSGs have been tabulated in Supplementary Information S2 and are summarized in Fig. 1a. While exhibiting one-to-one correspondence with 1421 MSGs, 1421 collinear SSGs manifest more spin symmetries, including spin $SO(2)$, $TU_n(\pi)$ and $\{U_n(\pi)||A\}$, which are crucial for more band degeneracies beyond the regime of MSGs (see a detailed comparison in

Supplementary Information S1). We list the SSGs of all collinear magnets in MAGNDATA in our online database FINDSPINGROUP⁵⁶.

Workflow

Figure 2a outlines the procedure to obtain all types of unconventional magnons and their realization in collinear magnets documented in MAGNDATA. Starting from 1421 collinear SSGs, we establish the position-space description of collinear SSGs, where the spin site groups for all spin Wyckoff positions can be defined and characterized by 90 collinear spin point groups. Among these groups, only 32 FM spin point groups support nonzero magnetic moments, resulting in a reduction of the total number of spin Wyckoff positions from 12481 to 7936. Meanwhile, we introduce a momentum-space description for collinear SSGs, exhausting the Brillouin zones and high-symmetry k -points using 24 mapped centrosymmetric symmorphic space groups. Subsequently, by employing Zak's method⁵⁸, we derive the irreducible little co-representations of magnons in collinear SSGs and enumerate all band representations hosting unconventional magnons. Finally, we construct $k \cdot p$ effective models around the degenerate points and evaluate the node topology characterized by chiral charge or monopole charge, identifying all unconventional magnons beyond the scope of MSGs. The general positions, Wyckoff positions, spin site groups, spin Brillouin zones, k -little groups, and magnon band representations for all collinear SSGs are available in our online database FINDSPINGROUP.

For material realization, we adopt MAGNDATA database that contains more than 2000 commensurate magnetic structures determined by neutron scattering measurements. By spin group symmetry identification, we filter out 1224 collinear magnets with their SSGs and spin Wyckoff positions. According to the corresponding band representations, we identify 498 materials hosting unconventional magnons, including 5 FMs, 17 FiMs and 476 AFMs, which can be further classified into 56 PT AFMs, 203 altermagnets and 217 $U\tau$ AFMs. After excluding magnetic structures with fractional occupancy or more than 80 atoms in the spin primitive cell, we perform density functional theory (DFT) and Wannier projection calculations on 348 materials.

After filtering out the cases failing of convergence and Wannierization, we obtain the bilinear magnetic exchange coefficients of 223 collinear magnets by using TB2J code. The magnon band structures of the Heisenberg spin Hamiltonians are calculated by the linear spin wave theory (LSWT). Specifically, Holstein-Primakoff transformation $S^+ \approx \sqrt{2S}a, S^- \approx \sqrt{2S}a^\dagger, S^z = S - a^\dagger a$ connects the magnon creation a^\dagger (annihilation a) operator with the electron annihilation S^- (creation S^+) operator⁵⁹. Finally, we obtain the unconventional magnons and corresponding irreducible co-representations (co-irreps) in 203 collinear magnets, while the magnon Hamiltonians of the other 20 systems are negative definite, leading to the magnetic instability.

Catalog of unconventional magnons

The bases of magnon bands S^\pm transform as the irreducible representations (irreps) of the spin site groups of the magnetic ions. For collinear magnets, the spin site group always have $SO(2)$ spin rotation symmetry, S^\pm thus transform as $m_s = \pm 1$ irreps of $SO(2)$ in spin space, while the real-space part only provides the identity irrep for S^\pm . As a result, there are three main types of symmetry resulting in extra degeneracies of magnon bands: (i) Unitary spin-space symmetry (USS): the combination of $SO(2)$ with unitary $\{U_n(\pi)||A\}$ symmetry pairs two conjugated one-dimensional (1D) irreps for S^\pm into a two-dimensional (2D) irrep in spin space. (ii) Antiunitary spin-space symmetry (ASS): combination of $SO(2)$ with antiunitary $\{T||A\}$ pairs two conjugated 1D irreps for S^\pm into a 2D co-irrep in spin space. (iii) Antiunitary real-space symmetry (ARS): antiunitary $\{TU_n(\pi)||E\}$ symmetry pairs two conjugated irreps of real-space operations (see Methods).

We next note several features of the magnon band degeneracies based on the co-irreps of collinear SSG: i) Despite the absence of T , type-I SSGs have the same band degeneracy and topology with the corresponding space group G combining T due to $\{TU_n(\pi)||E\}$ symmetry. This is also applicable in searching electronic orbital multiplets of collinear FM⁶⁰. ii) For collinear SSGs describing AFM, magnon band structures are doubly degenerate throughout the Brillouin zone for all type-II and type-IV SSGs, because of ASS $\{T||P\}$ and USS $\{U_n(\pi)||\tau\}$ at an arbitrary k point, respectively. iii) The topological charges at nodal points or lines formed by two opposite-spin branches are opposite for type-II SSGs, but identical for type-IV SSGs.

iv) Magnon band structures with type-III SSGs show AFM-induced chirality splitting, the magnonic analog of spin splitting in altermagnets^{39,61}. Therefore, the unconventional magnons can be classified into five categories: (1) topological charge-neutral ($C = 0$) quasiparticles, including duodecupole, octupole, sextupole and triple magnons; (2) chiral quasiparticles ($C > 0$), including C-4 octupole, C-4 sextupole, C-8 Dirac and C-2 triple magnons; (3) octupole nodal line magnon; (4) quadruple nodal plane magnon; and (5) altermagnetic-splitting chiral magnon. The correspondence between co-irreps and unconventional magnons in all collinear SSGs is provided in Supplementary Information S3.

Figure 2b summarizes the statistics of material candidates hosting the five categories of unconventional magnons. Notably, about 40% of the collinear magnets possess at least one type of unconventional magnons. The two major types are quadruple nodal plane magnon (22.34%) and altermagnetic chiral magnon (16.45%). This is consistent with that the proportion of altermagnets and $U\tau$ AFMs is relatively large in collinear magnets with unconventional magnons. In Table I we list some representative materials with their SSGs, co-irreps, and magnon node topology, where the diagnosis results of all 498 materials with unconventional magnon are provided in Supplementary Information S4. Specifically, we note that even the total topological charges of the Dirac and sextuple points in some PT AFMs are zero²², their node topology can be characterized by a nonzero C_2 topological number because the composite Weyl or triple points of the two spin channels host opposite topological charges (see Methods). Therefore, breaking $\{U_n(\pi)\|P\}$ symmetry, e.g., by an external magnetic field, could be feasible for the detection of spatially resolved thermal conductivity, i.e., “hidden” magnon thermal Hall effect.

Representative materials with unconventional magnons

Now we present calculated materials manifesting various unconventional magnons in each type of SSGs, including their degeneracy and node topology. The calculated magnon band structures of all the 203 candidates are provided in Supplementary Information S5. We begin with sextuple and triple points in type-I collinear SSG $I\bar{4}13^1d^{\infty}m1$ in FM Gd_4Sb_3 (Figs. 3a-3c). Within the regime of MSG, since that collinear magnets cannot be cubic, triple or sextuple magnons are thus absent. However, we find triple magnons at the Γ point, indicating that the SSG maintains the cubic nature of the lattice. In addition, due to the ARS $\{TU_n(\pi)\|C_{2z}|\tau_{y/2}\}$, two triple

magnons stick together forming a sextuple magnon at the boundary of Brillouin zone (H point). This is a typical case where the decoupled spin and space rotations in type-I SSGs provide more fertile platform for quasiparticles than MSGs. We note that similar ARS was found to protect the two-fold nodal plane in collinear FM Gd³².

Compared with the collinear FM, spin space can lead to additional degeneracy by USS and/or ASS in collinear AFM. The presented example is PT AFM Cu₃TeO₆ (Figs. 3d-3f), whose magnon dispersion were measured by inelastic neutron scattering experiments^{9,31}. Specifically, the magnon bands are doubly degenerate throughout the whole Brillouin zone, with several sextuple and Dirac magnons identified at the Γ , P and H points. These features are all beyond the regime of MSG, where the corresponding MSG $R\bar{3}'$ predicts non-degenerate band at an arbitrary k point and at most two-fold band crossings at any high-symmetry points (see Supplementary Information S7). In sharp contrast, these band degeneracies are perfectly described using co-irreps of the type-II cubic SSG $I\bar{1}a\bar{1}\bar{3}^{\infty m}1$. As discussed above, the ASS $\{T\|P\}$ at arbitrary k points protects doubly degenerate band throughout the Brillouin zone²². Similar doubly degenerate magnon modes are also experimentally observed in CrI₃, CoTiO₃^{7,62}. Furthermore, the little group $\bar{1}m\bar{1}\bar{3}^{\infty m}1$ allows sextuple magnons at Γ , P and H points, among which Γ and H manifest C_2-2 topological charge and thus the hidden magnon thermal Hall effect (Table I). By symmetry diagnosis, we predict that such hidden effects could also be detected in K_yFe_{2-x}Se₂, a widely-explored iron-based superconductor^{63,64}. We further note that the highest dimension of the symmetry-protected magnon bands in type-II SSGs is twelve. A representative example is the R point in experimentally synthesized Pr₅Mo₃O₁₆, where a collinear AFM order is implemented (Supplementary Information S7).

Another interesting case is the octuple magnon, which is found at the A point in type-III SSG $P\bar{1}\bar{6}\bar{1}2^1c^{\infty m}1$, in FeS (Figs. 3g-3i). Such an octuple magnon is also the synergistic effect of the ASS ($\{U_n(\pi)\|m_z|\tau_{z/2}\}$) and ARS ($\{T\|2_x|0\}$). Moreover, the bands off the high-symmetry point are nondegenerate, leading to AFM-induced magnon chirality splitting along, e.g., Γ -A and A-K directions. We expect that magnon chirality splitting in collinear AFM can lead to the appearance of non-zero Berry curvature, magnon orbital angular momentum, and magnon nonlinear thermal Hall in the absence of SOC, which will further expand the scope of relevant field of spintronics⁶⁵⁻⁶⁸. We list all the 203 diagnosed altermagnets from MAGNDATA in

Supplementary Information S4.

The magnon quasiparticles carry various topological charges, some of which are absent in all encyclopedias of MSGs⁶⁹⁻⁷¹ but protected by SSG symmetries. One striking case is the charge-4 (C-4) octuple magnons (Figs. 3j-3l) in collinear $\text{Fe}_{0.35}\text{NbS}_2$ with a type-IV SSG $P_a^1 2_1^1 2_1^1 2_1^{\infty m} 1$. Due to the $\{U_n(\pi) \| E | \tau\}$ and ARS $\{T \| C_z(\pi) | \tau_{x/2}\}$ of the little group of $k_z = \pi$ plane, the magnon bands form quadruple Z-U-R-T nodal plane and octuple quasiparticle at the R point. Different from type-II SSGs, the sign of Berry curvature from the two pairs of four-fold degenerate bands connected by $\{U_n(\pi) \| E | \tau\}$ are identical for type-IV SSGs, resulting in C-4 octuple magnons as the superposition of two C-2 Dirac points at R (see Supplementary Information S7). Furthermore, three perpendicular k-planes ($k_x, k_y, k_z = \pi$) intersecting at the R point form a quadruple nodal plane network (see Supplementary Information S7). We predict plenty cases of magnon band topology such as C-4 sextuple and C-8 Dirac magnons as summarized in Supplementary Information S4.

SOC effects

To evaluate the applicability of collinear SSGs in diagnosing unconventional magnons, we fully consider SOC effects by calculating the bilinear magnetic exchange interactions, including antisymmetric DM interaction (D), Kitaev interaction (K), and symmetric anisotropy (F), and compare them with the isotropic Heisenberg exchange interaction (J) in 223 candidate materials. Comparing with SOC-free calculations, the high-throughput SOC calculations yield over 30 times of computational costs. Notably, single-ion anisotropy is excluded in our analysis because in collinear magnets it does not affect the symmetry of the magnon Hamiltonian, the band representations and the nodal topology (see Supplementary Information S7). Table II shows that in 82% of the calculated collinear magnets, DM interaction, Kitaev interaction, and symmetric anisotropy are at least an order of magnitude smaller than the Heisenberg interaction, indicating the validity of SSG for these systems. Specifically, 87% of the $3d$ and $4d$ magnets are dominated by Heisenberg interactions, while the remaining ones possess strong DM interactions, such as the reported altermagnet $\text{Fe}_2\text{Mo}_3\text{O}_8$ with DM interaction-induced magnon polaron⁷². In addition, the half-filled $4f$ magnets are also

largely compatible with the framework of SSGs, such as Gd^{3+} in GdAlO_3 and GdAgSn . However, the $5d$ and $5f$ magnets failed due to the strong DM or Kitaev interactions. These results indicate that SSG serves as an ideal framework for describing magnon band nodes in most $3d$, $4d$ and $4f$ collinear magnets. Detailed information regarding the calculated exchange interactions for 223 candidates is available in Supplementary Information S6.

For collinear magnets, there exists an effective time-reversal symmetry $TU_n(\pi)$ that squares to one. Consequently, magnons in collinear magnets fall into the class AI in the tenfold way, which do not support strong topological insulating phase in 3D^{73,74}. Recent studies show that SOC-free weak topological insulators could exist in altermagnets⁷⁵. On the other hand, under nonlinear spin wave theory, the introduction of magnon-magnon interaction does not break the $\text{SO}(2)$ symmetry in collinear magnets. Thus, it does not change the band degeneracy, while it may cause band renormalization⁷⁶. However, adding SOC term to collinear spin Hamiltonian typically opens a small gap, sometimes rendering the emergence of class AII and \mathbb{Z}_2 gapped topological phase. For example, the introduction of DM interaction in pyrochlore, honeycomb and kagome FMs can transform Dirac magnons into topological magnon bands⁷⁷⁻⁷⁹. In this case, the description of SSGs is still useful in that it can be used to search for the SOC-induced small gap, which is often the prerequisite of magnon topological materials, such as Chern insulators and axion insulators. Furthermore, the incorporation of DM interaction and magnon-magnon interactions can cause multiple topological phase transitions.^{80,81} Overall, understanding the evolution from node topology to band topology with the introduction of SOC effect and its impact on magnon transport will be valuable for the development of magnon-based spintronic devices, and is left for future studies.

Discussion

Importantly, we emphasize that while our focus is on magnon systems, the main results of unconventional quasiparticles originated from band degeneracies can be straightforwardly applied to electronic systems. In the framework of (magnetic) space group, the double-valued representation of spin-1/2 fermions requires the so-called

double group to describe an additional -1 phase of 2π rotation. In sharp contrast, the particularity of collinear SSGs renders that the dimension of the band representations for both fermions and bosons remains invariant within 4π rotation. This is because the infinite spin-only group $SO(2)$ has the double-covering group of itself, and can thus be regarded as either a single group or a double group. Therefore, $SO(2)$ always provides 1D irreps labeled by spin angular momentum $m_s = \pm 1/2$ for electrons and $m_s = \pm 1$ for magnons. The only difference between fermions and bosons in collinear SSGs occurs solely within the phase in irrep matrices.

The main outcome of this work is twofold. First, we present a comprehensive representation theory of 1421 collinear SSGs, which includes the Wyckoff positions, spin Brillouin zones, and band representations associated with each wavevector. Such framework allows for the full tabulation of unconventional magnons beyond the MSGs. Second, we provide a dictionary of over 200 candidate materials that host unconventional magnons, identified through high-throughput calculations. The integration of SSGs and the collinear magnets listed in the MAGNDATA database facilitates efficient and systematic characterization of magnons exhibiting nontrivial nodal topology. By virtue of this, the unconventional magnons have the potential to host topologically protected, uncharged surface states, leaving fruitful transport and neutron scattering signatures for experiments.

Methods

Band representation theory for SSGs. Band representations are constructed from atomic limit as introduced by Zak⁵⁸. Firstly, we construct the spin site group G_{SSG}^q of the spin space group G_{SSG} , the corresponding character table and the irreps of orbit basis $\rho_{S_{\pm}}^q$, where q is any point in the unit cell of magnetic lattice. Among these spin site groups, only 32 FM spin point groups can support nonzero magnetic moments and carry magnon. Secondly, to induce full band representations $\rho_{S_{\pm}} = \rho_{S_{\pm}}^q \uparrow G_{SSG}$, we seek a coset decomposition of G_{SSG}^q in G_{SSG} . All orbits of the Wyckoff position $\{q_{\alpha} = g_{\alpha}q_1 | q_{\alpha} \in H_{SS}\}$, $\alpha = 1, 2, \dots, n$ with multiplicity n of the Wyckoff position are derived. The spin space group element g_{α} , combined with the translation \mathbb{T} , generate the decomposition of G_{SSG} with respect to the G_{SSG}^q :

$$G_{SSG} = \bigcup_{\alpha} g_{\alpha} (G_{SSG}^q \rtimes \mathbb{T})$$

The ingredients for induction are

$$\chi_{\rho_{S_{\pm}^k}}(g) = \begin{cases} \sum_{\alpha} e^{-i[R(g)k \cdot t_{\alpha\alpha}]} \chi_{\rho_{S_{\pm}^k}}(g_{\alpha}^{-1} \{E|E|-t_{\alpha\alpha}\} g g_{\alpha}) & g \in G_{SS}^q \\ 0 & g \notin G_{SS}^q \end{cases}$$

where $t_{\alpha\alpha} = gq_{\alpha} - q_{\alpha}$. Thirdly, since we concentrate on the symmetry of different k point, we subduce $\rho_{S_{\pm}^k}$ into different little groups $\rho_{S_{\pm}^k} = \rho_{S_{\pm}^k} \downarrow G_{SSG}^k$ based on the Fourier transformation. In this step, the character table of the unitary part of G_{SSG}^k is also constructed. At last, we perform sum rules²¹ to account for the introduction of anti-unitary operations and the band representation $\rho_{S_{\pm}^k}$ in SBZ is determined. The construction of band representation for SSG $I^{\bar{1}}a^{\bar{1}}\bar{3}^{\infty m}1$ (Cu_3TeO_6 case) can be found in Supplementary Information S7.

Two mechanisms of extra twofold degeneracy provided by spin space. For collinear AFM, G_{SSG} have the form of $(\{E|G_{\uparrow}\} + \{U_{\mathbf{n}}(\pi)||AG_{\uparrow}\}) \times Z_2^K \rtimes SO(2)$. Here we briefly show how the combination of $SO(2)$ spin symmetry with $\{U_{\mathbf{n}}(\pi)||A\}$ or $\{T||A\}$ will pair two 1D representations into 2D irreps for S^{\pm} in spin space.

Despite the pure space rotations (G_{\uparrow}^k) and pure spin rotations from $SO(2)$ symmetry in the little group G_{SSG}^k , three symmetry operations account for the twofold degeneracy in spin space, including $\{U_{\mathbf{n}}(\pi)||A\}$, $\{T||A\}$ and $\{TU_{\mathbf{n}}(\pi)||E\}$. Here we show how these operations acting with the $U_{\mathbf{z}}(\phi)$ in the $\{S^+, S^-\}$ basis.

The matrix representations of spin rotations and the time reversal are written as:

$$D(U_{\mathbf{z}}(\phi)) = \begin{pmatrix} e^{-i\phi} & 0 \\ 0 & e^{i\phi} \end{pmatrix}, D(U_{\mathbf{x}}(\pi)) = \begin{pmatrix} 0 & 1 \\ 1 & 0 \end{pmatrix}, D(T) = \begin{pmatrix} 0 & -1 \\ -1 & 0 \end{pmatrix} K,$$

where K is the complex conjugation operator, and we use $\mathbf{n} = x$.

For $\{U_{\mathbf{x}}(\pi)||A\}$:

$$\begin{aligned} & \{U_{\mathbf{x}}(\pi)||A\} \{U_{\mathbf{z}}(\phi)||E\} (\{U_{\mathbf{x}}(\pi)||A\})^{-1} = \{U_{\mathbf{z}}(-\phi)||E\} \\ & \Rightarrow (\{E|G_{\uparrow}^k\} + \{U_{\mathbf{n}}(\pi)||AG_{\uparrow}^k\}) \rtimes SO(2) \cong \{E|G_{\uparrow}^k\} \times D_{\infty} \end{aligned}$$

where D_{∞} provide 2D irreps for S^{\pm} .

For $\{T||A\}$:

$$(\{T\|A\}\{U_z(\phi)\|E\})^2 \begin{pmatrix} \psi_{i,S^+}(k) \\ \psi_{i,S^-}(k) \end{pmatrix} = \begin{pmatrix} e^{2i\phi}\psi_{i,S^+}(k) \\ e^{-2i\phi}\psi_{i,S^-}(k) \end{pmatrix}$$

where the time reversal binds two conjugated 1D irreps in spin space into one 2D co-irrep.

For $\{TU_x(\pi)\|E\}$:

$$(\{TU_x(\pi)\|E\}\{U_z(\phi)\|E\})^2 \begin{pmatrix} \psi_{i,S^+}(k) \\ \psi_{i,S^-}(k) \end{pmatrix} = \begin{pmatrix} \psi_{i,S^+}(k) \\ \psi_{i,S^-}(k) \end{pmatrix}$$

$\{TU_x(\pi)\|E\}$ cannot contribute to the new degeneracy.

Therefore, we can conclude that both $\{U_n(\pi)\|A\}$ and $\{T\|A\}$ can lead to the emergence of 2D irreps in spin space.

Density functional theory (DFT) calculations. All DFT calculations herein are performed using projector augmented wave method, implemented in Vienna ab initio simulation package (VASP)^{82,83}. The generalized gradient approximation of the Perdew-Burke-Ernzerhof-type exchange-correlation potential⁸⁴ is adopted. To include the effect of electron correlation, the DFT+U approach within the rotationally invariant formalism⁸⁵ were performing with $U_{\text{eff}} = 6.0$ eV for Gd 4f (Gd₄Sb₃) and $U_{\text{eff}} = 1.0$ eV for Fe 3d (FeS, Fe_{0.35}NbS₂). Tight-binding models are constructed from DFT bands using the WANNIER90 package^{86,87}, and then the TB2J code⁸⁸ is used to extract the magnetic exchange parameters. In high-throughput calculations, the selection of U_{eff} values is based on the reported value from literature, which are provided in Supplementary Information S5 for each material. Detailed parameters and cutoffs of Heisenberg exchange interactions for calculating the magnon band structure can be found in the Supplementary Information S6.

Magnon band structure calculations. The magnon band structure are all calculated using the LSWT and the Heisenberg spin Hamiltonian. The ground state spin Hamiltonian can be changed into quadratic Hamiltonian by performing the Holstein-Primakoff transformation and Fourier transformation:

$$H = \sum_k \psi^\dagger(k)H(k)\psi(k)$$

where $\psi^\dagger(k) = (a_{k1}^\dagger \dots a_{km}^\dagger a_{-k1} \dots a_{-km})^T$, $H(k) = \begin{pmatrix} h(k) & g(k) \\ g(k)^\dagger & h(-k)^T \end{pmatrix}$

$$h(k)_{ab} = S \left[\sum_{R_{ij}} (\alpha_{ab} J_{\tau_a, \tau_b + R_{ij}}) \cdot e^{ikR_{ij}} - \delta_{ab} \sum_{R_{ij}, c} (\gamma_{ac} J_{\tau_a, \tau_c + R_{ij}}) \right]$$

$$g(k)_{ab} = S \sum_{R_{ij}} (\lambda_{ab} J_{\tau_a, \tau_b + R_{ij}}) \cdot e^{ikR_{ij}}$$

where δ_{ab} is the Kronecker delta, R and τ represent the lattice translation vector and the position of magnetic ions in the lattice basis, respectively. When \vec{S}_a is parallel with \vec{S}_b , $\alpha_{ab} = 1, \gamma_{ab} = 1, \lambda_{ab} = 0$; when \vec{S}_a is antiparallel with \vec{S}_b , $\alpha_{ab} = 0, \gamma_{ab} = -1, \lambda_{ab} = -1$.

Based on above, the eigenvalues and eigenvectors of magnon Hamiltonian can be calculated by diagonalizing $H(k) \cdot I_-$, where $I_- = \begin{pmatrix} I_m & 0 \\ 0 & -I_m \end{pmatrix}$, and I_m is the m -directional identity matrix.

Topological charges. We characterize the topology of the degenerate point by calculating the topological charge. For nodal point, we calculate the Wilson loops on a sphere enclosing the nodal point^{89,90}:

$$W(\theta) = \oint A(k) dk$$

where θ is the polar angle of the sphere, $A(k) = i\langle \psi(k) | \nabla | \psi(k) \rangle$ is the Berry connection.

Now we show the different symmetry operations on $A(k)$:

$$PA(k) = -A(-k), TA(k) = A(-k), UA(k) = A(k)$$

As a result, the topological charge is zero at P -symmetric k points since $PW(\theta) = W(\pi - \theta)$, where Wilson loop is symmetric about the $\theta = \pi/2$ plane. This conclusion can be generalized to PC_n -invariant k point, where C_n is any proper space rotation. However, the time reversal T and spin rotation U does not give any constraints on the topological charge.

For collinear FMs, when the k -little group is chiral, it can host a nonzero topological charge. For collinear AFMs, the magnon Hamiltonian can be separated into two spin channels with spin angular momentum $S = \pm 1$, the two degenerate spin channels should be connected by TA or UA . If the k -little sublattice group G_\uparrow^k is chiral, it can

host a nonzero topological charge C_{\uparrow} in the spin up channel. The two spin channels can possess identical or opposite topological charges when the two sublattice are connected by proper or improper A . In the former, the topological charge will be doubled as $C = 2C_{\uparrow}$, while $C = 0$ in the latter. For the compensated charge with improper A , we can define a monopole charge $C_2 = (C_{\uparrow} - C_{\downarrow})/2$.

Therefore, the nodal points of two degenerate branches possess opposite (identical) topological charges for type-II (IV) SSGs due to the PT ($U\tau$) symmetry in the whole spin Brillouin zone. For type-III SSGs, if G_{\uparrow}^k is chiral and the k -little group G^k contain TA and UA operation, the two magnon branches will degenerate with doubled or compensated topological charge when A is proper or improper. However, when the k -little group does not contain TA and UA operation, the two magnon branches will split and the sign of topological charge in two channels is irrelevant.

Detailed information about the nonzero topological charges of magnonic irreps in collinear SSGs at symmetry-protected degeneracies is provided on our online program FINDSPINGROUP⁵⁶.

Acknowledgements

This work was supported by National Key R&D Program of China under Grant No. 2020YFA0308900, the National Natural Science Foundation of China under Grant No. 12274194, Guangdong Provincial Key Laboratory for Computational Science and Material Design under Grant No. 2019B030301001, Shenzhen Science and Technology Program (Grants No. RCJC20221008092722009 and No. 20231117091158001), Innovative Team of General Higher Educational Institutes in Guangdong Province (No. 2020KCXTD001), the Science, Technology and Innovation Commission of Shenzhen Municipality (No. ZDSYS20190902092905285), the Open Fund of the State Key Laboratory of Spintronics Devices and Technologies under Grant No. SPL-2407 and Center for Computational Science and Engineering of Southern University of Science and Technology.

References

1. Bradlyn, B. et al. Topological quantum chemistry. *Nature* **547**, 298 (2017).

2. Kruthoff, J. et al. Topological Classification of Crystalline Insulators through Band Structure Combinatorics. *Phys. Rev. X* **7**, 041069 (2017).
3. Elcoro, L. et al. Magnetic topological quantum chemistry. *Nat. Commun.* **12**, 5965 (2021).
4. Zhang, T. et al. Catalogue of Topological Electronic Materials. *Nature* **566**, 475 (2019).
5. Vergniory, M. G. et al. A complete catalogue of high-quality topological materials. *Nature* **566**, 480 (2019).
6. Tang, F., Po, H. C., Vishwanath, A. & Wan, X. Comprehensive search for topological materials using symmetry indicators. *Nature* **566**, 486 (2019).
7. Yuan, B. et al. Dirac Magnons in a Honeycomb Lattice Quantum XY Magnet CoTiO_3 . *Phys. Rev. X* **10**, 011062 (2020).
8. Chen, L. et al. Topological Spin Excitations in Honeycomb Ferromagnet CrI_3 . *Phys. Rev. X* **8**, 041028 (2018).
9. Bao, S. et al. Discovery of coexisting Dirac and triply degenerate magnons in a three-dimensional antiferromagnet. *Nat. Commun.* **9**, 2591 (2018).
10. Li, F.-Y. et al. Weyl magnons in breathing pyrochlore antiferromagnets. *Nat. Commun.* **7**, 12691 (2016).
11. Mook, A., Henk, J. & Mertig, I. Tunable Magnon Weyl Points in Ferromagnetic Pyrochlores. *Phys. Rev. Lett.* **117**, 157204 (2016).
12. Su, Y., Wang, X. S. & Wang, X. R. Magnonic Weyl semimetal and chiral anomaly in pyrochlore ferromagnets. *Phys. Rev. B* **95**, 224403 (2017).
13. Hwang, K., Trivedi, N. & Randeria, M. Topological Magnons with Nodal-Line and Triple-Point Degeneracies: Implications for Thermal Hall Effect in Pyrochlore Iridates. *Phys. Rev. Lett.* **125**, 047203 (2020).
14. McClarty, P. A. Topological Magnons: A Review. *Annu. Rev. Condens. Matter Phys.* **13**, 171 (2022).
15. Kondo, H. & Akagi, Y. Dirac Surface States in Magnonic Analogs of Topological Crystalline Insulators. *Phys. Rev. Lett.* **127**, 177201 (2021).
16. Li, S. & Nevidomskyy, A. H. Topological Weyl magnons and thermal Hall effect in

- layered honeycomb ferromagnets. *Phys. Rev. B* **104**, 104419 (2021).
17. Cheng, R., Okamoto, S. & Xiao, D. Spin Nernst Effect of Magnons in Collinear Antiferromagnets. *Phys. Rev. Lett.* **117**, 217202 (2016).
 18. Zyuzin, V. A. & Kovalev, A. A. Spin Hall and Nernst effects of Weyl magnons. *Phys. Rev. B* **97**, 174407 (2018).
 19. Hetényi, B., Mook, A., Klinovaja, J. & Loss, D. Long-distance coupling of spin qubits via topological magnons. *Phys. Rev. B* **106**, 235409 (2022).
 20. Baltz, V. et al. Antiferromagnetic spintronics. *Rev. Mod. Phys.* **90**, 015005 (2018).
 21. Dimmock, J. O. & Wheeler, R. G. Symmetry Properties of Wave Functions in Magnetic Crystals. *Phys. Rev.* **127**, 391 (1962).
 22. Li, K. et al. Dirac and Nodal Line Magnons in Three-Dimensional Antiferromagnets. *Phys. Rev. Lett.* **119**, 247202 (2017).
 23. Karaki, M. J. et al. An efficient material search for room-temperature topological magnons. *Sci. Adv.* **9**, eade7731 (2023).
 24. Corticelli, A., Moessner, R. & McClarty, P. A. Identifying and Constructing Complex Magnon Band Topology. *Phys. Rev. Lett.* **130**, 206702 (2023).
 25. Dzyaloshinsky, I. A thermodynamic theory of “weak” ferromagnetism of antiferromagnetics. *J. Phys. Chem. Solids* **4**, 241 (1958).
 26. Moriya, T. Anisotropic superexchange interaction and weak ferromagnetism. *Phys. Rev.* **120**, 91 (1960).
 27. Brinkman, W. Magnetic Symmetry and Spin Waves. *J. Appl. Phys.* **38**, 939 (1967).
 28. Brinkman, W. F. & Elliott, R. J. Theory of spin-space groups. *Proc. R. Soc. A* **294**, 343 (1966).
 29. Liu, P. et al. Spin-Group Symmetry in Magnetic Materials with Negligible Spin-Orbit Coupling. *Phys. Rev. X* **12**, 021016 (2022).
 30. Corticelli, A., Moessner, R. & McClarty, P. A. Spin-space groups and magnon band topology. *Phys. Rev. B* **105**, 064430 (2022).
 31. Yao, W. et al. Topological spin excitations in a three-dimensional antiferromagnet. *Nat. Phys.* **14**, 1011 (2018).
 32. Scheie, A. et al. Dirac Magnons, Nodal Lines, and Nodal Plane in Elemental

- Gadolinium. *Phys. Rev. Lett.* **128**, 097201 (2022).
33. Scheie, A. et al. Spin-exchange Hamiltonian and topological degeneracies in elemental gadolinium. *Phys. Rev. B* **105**, 104402 (2022).
 34. Zelezny, J., Zhang, Y., Felser, C. & Yan, B. Spin-Polarized Current in Noncollinear Antiferromagnets. *Phys. Rev. Lett.* **119**, 187204 (2017).
 35. Liu, P., Zhang, A., Han, J. & Liu, Q. Chiral Dirac-like fermion in spin-orbit-free antiferromagnetic semimetals. *The Innovation* **3**, 100343 (2022).
 36. Yang, J., Liu, Z.-X. & Fang, C. Symmetry invariants in magnetically ordered systems having weak spin-orbit. Preprint at *arXiv* <https://arxiv.org/abs/2105.12738> (2022).
 37. Šmejkal, L., Sinova, J. & Jungwirth, T. Beyond Conventional Ferromagnetism and Antiferromagnetism: A Phase with Nonrelativistic Spin and Crystal Rotation Symmetry. *Phys. Rev. X* **12**, 031042 (2022).
 38. Ma, H.-Y. et al. Multifunctional antiferromagnetic materials with giant piezomagnetism and noncollinear spin current. *Nat. Commun.* **12**, 2846 (2021).
 39. Šmejkal, L., Sinova, J. & Jungwirth, T. Emerging Research Landscape of Altermagnetism. *Phys. Rev. X* **12**, 040501 (2022).
 40. Hayami, S., Yanagi, Y. & Kusunose, H. Momentum-Dependent Spin Splitting by Collinear Antiferromagnetic Ordering. *J. Phys. Soc. Jpn.* **88**, 123702 (2019).
 41. Yuan, L.-D. et al. Giant momentum-dependent spin splitting in centrosymmetric low-*Z* antiferromagnets. *Phys. Rev. B* **102**, 014422 (2020).
 42. Guo, P. J. et al. Eightfold Degenerate Fermions in Two Dimensions. *Phys. Rev. Lett.* **127**, 176401 (2021).
 43. Shao, D. F. et al. Spin-neutral currents for spintronics. *Nat. Commun.* **12**, 7061 (2021).
 44. Bai, H. et al. Observation of Spin Splitting Torque in a Collinear Antiferromagnet RuO₂. *Phys. Rev. Lett.* **128**, 197202 (2022).
 45. Bai, H. et al. Efficient Spin-to-Charge Conversion via Altermagnetic Spin Splitting Effect in Antiferromagnet RuO₂. *Phys. Rev. Lett.* **130**, 216701 (2023).
 46. Bose, A. et al. Tilted spin current generated by the collinear antiferromagnet

- ruthenium dioxide. *Nat. Electron.* **5**, 267 (2022).
47. Feng, Z. et al. An anomalous Hall effect in altermagnetic ruthenium dioxide. *Nat. Electron.* **5**, 735 (2022).
 48. Shao, D. F. et al. Neel Spin Currents in Antiferromagnets. *Phys. Rev. Lett.* **130**, 216702 (2023).
 49. Zhu, Y.-P. et al. Observation of plaid-like spin splitting in a noncoplanar antiferromagnet. *Nature* **626**, 523-528 (2024).
 50. Krempaský, J. et al. Altermagnetic lifting of Kramers spin degeneracy. *Nature* **626**, 517-522 (2024).
 51. Xiao, Z. et al. Spin space groups: full classification and applications. *Phys. Rev. X* **14**, 031037 (2024).
 52. Chen, X. et al. Enumeration and representation theory of spin space groups. *Phys. Rev. X* **14**, 031038 (2024).
 53. Jiang, Y. et al. Enumeration of spin-space groups: Toward a complete description of symmetries of magnetic orders. *Phys. Rev. X* **14**, 031039 (2024).
 54. Ghorashi, S. A. A., Hughes, T. L. & Cano, J. Altermagnetic routes to Majorana modes in zero net magnetization. *Phys. Rev. Lett.* **133**, 106601 (2024).
 55. Gallego, S. V. et al. MAGNDATA: towards a database of magnetic structures. I. The commensurate case. *J. Appl. Crystallogr.* **49**, 1750 (2016).
 56. <https://findspingroup.com/>.
 57. Litvin, D. B. Spin point groups. *Acta Crystallogr. A* **33**, 279 (1977).
 58. Zak, J. Band representations of space groups. *Phys. Rev. B* **26**, 3010 (1982).
 59. Holstein, T. & Primakoff, H. Field Dependence of the Intrinsic Domain Magnetization of a Ferromagnet. *Phys. Rev.* **58**, 1098 (1940).
 60. Li, J. et al. Designing light-element materials with large effective spin-orbit coupling. *Nat. Commun.* **13**, 919 (2022).
 61. Šmejkal, L. et al. Chiral magnons in altermagnetic RuO₂. *Phys. Rev. Lett.* **131**, 256703 (2023).
 62. Cenker, J. et al. Direct observation of two-dimensional magnons in atomically thin CrI₃. *Nat. Phys.* **17**, 20 (2020).

63. Pomjakushin, V. Y. et al. Room temperature antiferromagnetic order in superconducting $X_y\text{Fe}_{2-x}\text{Se}_2$ ($X = \text{Rb}, \text{K}$): a neutron powder diffraction study. *J. Phys.: Condens. Matter* **23**, 156003 (2011).
64. Yu, W. et al. ^{77}Se NMR study of the pairing symmetry and the spin dynamics in $\text{K}_y\text{Fe}_{2-x}\text{Se}_2$. *Phys. Rev. Lett.* **106**, 197001 (2011).
65. Liu, Y. et al. Switching magnon chirality in artificial ferrimagnet. *Nat. Commun.* **13**, 1264 (2022).
66. Neumann, R. R., Mook, A., Henk, J. & Mertig, I. Orbital Magnetic Moment of Magnons. *Phys. Rev. Lett.* **125**, 117209 (2020).
67. Fishman, R. S., Gardner, J. S. & Okamoto, S. Orbital Angular Momentum of Magnons in Collinear Magnets. *Phys. Rev. Lett.* **129**, 167202 (2022).
68. Go, G., An, D., Lee, H.-W. & Kim, S. K. Magnon Orbital Nernst Effect in Honeycomb Antiferromagnets without Spin–Orbit Coupling. *Nano Lett.* **24**, 5968 (2024).
69. Yu, Z. M. et al. Encyclopedia of emergent particles in three-dimensional crystals. *Sci. Bull.* **67**, 375 (2022).
70. Liu, G.-B. et al. Systematic investigation of emergent particles in type-III magnetic space groups. *Phys. Rev. B* **105**, 085117 (2022).
71. Zhang, Z. et al. Encyclopedia of emergent particles in type-IV magnetic space groups. *Phys. Rev. B* **105**, 104426 (2022).
72. Bao, S. et al. Direct observation of topological magnon polarons in a multiferroic material. *Nat. Commun.* **14**, 6093 (2023).
73. Altland, A. & Zirnbauer, M. R. Nonstandard symmetry classes in mesoscopic normal-superconducting hybrid structures. *Phys. Rev. B* **55**, 1142 (1997).
74. Xu, Q.-R. et al. Squaring the fermion: The threefold way and the fate of zero modes. *Phys. Rev. B* **102**, 125127 (2020).
75. Zhang, M.-H., Xiao, L. & Yao, D.-X. Topological magnons in a collinear altermagnet. Preprint at *arXiv* <https://arxiv.org/abs/2407.18379> (2024).
76. Pershoguba, S. S. et al. Dirac magnons in honeycomb ferromagnets. *Phys. Rev. X* **8**, 011010 (2018).

77. Zhang, L., Ren, J., Wang, J.-S. & Li, B. Topological magnon insulator in insulating ferromagnet. *Phys. Rev. B* **87**, 144101 (2013).
78. Mook, A., Henk, J. & Mertig, I. Edge states in topological magnon insulators. *Phys. Rev. B* **90**, 024412 (2014).
79. Owerre, S. A first theoretical realization of honeycomb topological magnon insulator. *J. Phys.: Condens. Matter* **28**, 386001 (2016).
80. Mook, A., Plekhanov, K., Klinovaja, J. & Loss, D. Interaction-stabilized topological magnon insulator in ferromagnets. *Phys. Rev. X* **11**, 021061 (2021).
81. Lu, Y.-S., Li, J.-L. & Wu, C.-T. Topological phase transitions of Dirac magnons in honeycomb ferromagnets. *Phys. Rev. Lett.* **127**, 217202 (2021).
82. Kresse, G. & Furthmüller, J. Efficient iterative schemes for *ab initio* total-energy calculations using a plane-wave basis set. *Phys. Rev. B* **54**, 11169 (1996).
83. Kresse, G. & Joubert, D. From ultrasoft pseudopotentials to the projector augmented-wave method. *Phys. Rev. B* **59**, 1758 (1999).
84. Perdew, J. P., Burke, K. & Ernzerhof, M. Generalized Gradient Approximation Made Simple. *Phys. Rev. Lett.* **77**, 3865 (1996).
85. Anisimov, V. I., Zaanen, J. & Andersen, O. K. Band theory and Mott insulators: Hubbard U instead of Stoner I. *Phys. Rev. B* **44**, 943 (1991).
86. Mostofi, A. A. et al. wannier90: A tool for obtaining maximally-localised Wannier functions. *Comput. Phys. Commun.* **178**, 685 (2008).
87. Marzari, N. et al. Maximally localized Wannier functions: Theory and applications. *Rev. Mod. Phys.* **84**, 1419 (2012).
88. He, X., Helbig, N., Verstraete, M. J. & Bousquet, E. TB2J: A python package for computing magnetic interaction parameters. *Comput. Phys. Commun.* **264**, 107938 (2021).
89. Yu, R. et al. Equivalent expression of Z_2 topological invariant for band insulators using the non-Abelian Berry connection. *Phys. Rev. B* **84**, 075119 (2011).
90. Berry, M. V. Quantal phase factors accompanying adiabatic changes. *Proc. R. Soc. A* **392**, 45 (1997).

Table I. | Summary of unconventional magnons identified in prototypical candidate materials. The superscript “†” represents that the nodal feature has been experimentally observed. The superscript “*” represents that the material is synthesized in experiment, but the magnetic structure is artificially imposed. “ $C-n$ ” means that the topological charge C is $|C| = n$. “ C_2-m ” means that the monopole charge $C_2 = (C_\uparrow - C_\downarrow)/2$ is $|C_2| = m$. DCP: duodecuple point; ONL: octuple nodal line; OP: octuple point; SP: sextuple point; QNP: Quadruple nodal plane; DP: Dirac point; TP: triple point.

| SSG | k | BRs at k | Type | Material |
|---|---|--|----------------------------------|--|
| 220.220.1.1 ($I^1\bar{4}^13^1d^{\infty m}1$) | H (1, 1, 1) Γ (0, 0, 0) | $H_4^S H_5^S(6)$ $\Gamma_4^S(3), \Gamma_5^S(3)$ | SP TP | Gd ₄ Sb ₃ (FM) |
| 227.227.1.1 ($F^1d^1\bar{3}^1m^{\infty m}1$) | Γ (0, 0, 0) | $\Gamma_5^{S,+}(3)$ | TP | Lu ₂ V ₂ O ₇ [†] (FM) |
| 212.212.1.1 ($P^14_3^13^12^{\infty m}1$) | Γ (0, 0, 0) | $\Gamma_4^S(3), \Gamma_5^S(3)$ | $C-2$ TP | LiFe ₅ O ₈ (FIM) |
| 218.222.1.1 ($P^1\bar{n}^1\bar{3}^1n^{\infty m}1$) | R (1/2, 1/2, 1/2) | $R_4^S R_5^S(12)$ | DCP | Pr ₅ Mo ₃ O ₁₆ [*] (PT AFM) |
| 199.206.1.1 ($I^1\bar{a}^1\bar{3}^{\infty m}1$) | Γ (0, 0, 0) H (1, 1, 1) | $\Gamma_4^S(6)$ $H_4^S(6)$ | C_2-2 SP | Cu ₃ TeO ₆ [†] (PT AFM) |
| 159.190.1.1 ($P^1\bar{6}^1\bar{2}^1c^{\infty m}1$) | A (0, 0, 1/2) | $A_3^S A_3^S(8)$ | OP | FeS (Altermagnet) |
| 62.63.2.1 ($P_B^1n^1m^1a^{\infty m}1$) | Q (1/2, 1/2, w) W ($u, v, 1/2$) | $Q_1^S Q_1^S(8)$ $W_1^S W_2^S(4)$ | ONL QNPL | Mn ₅ Si ₃ (U τ AFM) |
| 19.18.2.1 ($P_c^12_1^12_1^12_1^{\infty m}1$) | R (1/2, 1/2, 1/2) L (1/2, v, w) N ($u, 1/2, w$) W ($u, v, 1/2$) | $R_1^S R_1^S(8)$ $L_1 L_1(4)$ $N_1 N_1(4)$ $W_1 W_1(4)$ | $C-4$ OP QNPL net | Fe _{0.35} NbS ₂ (U τ AFM) |
| 195.197.2.1 ($P_I^12^13^{\infty m}1$) | Γ (0,0,0) Γ (0,0,0) R (1/2,1/2,1/2) | $\Gamma_2^S \Gamma_3^S(4)$ $\Gamma_4^S(6)$ $R_4^S(6)$ | $C-8$ DP $C-4$ SP $C-4$ SP | LaMn ₃ Cr ₄ O ₁₂ (U τ AFM) |

Table II. | Statistics of bilinear exchange interactions with SOC. The second columns present the number of collinear magnets classified by the outermost shell of magnetic ions in the first column. The third to fifth columns evaluate the number of materials in which the magnitude of DM (D), Kitaev (K), and anisotropic symmetric (Γ) terms does not exceed 10% of that of Heisenberg term (J), respectively. The last column gives the number of J dominated magnets, in which none of $|D|$, $|K|$ and $|\Gamma|$ exceeds 10% $|J|$.

| Magnetic ions | Materials | < 10% $ J $ | | | J dominated |
|---------------|-----------|-------------|-------|------------|---------------|
| | | $ D $ | $ K $ | $ \Gamma $ | |
| 3d | 194 | 175 | 182 | 189 | 169 |
| 4d | 7 | 5 | 5 | 6 | 5 |
| 4f | 12 | 11 | 10 | 11 | 9 |
| 5d | 6 | 1 | 0 | 3 | 0 |
| 5f | 4 | 1 | 0 | 3 | 0 |
| Total | 223 | 193 | 197 | 212 | 183 |

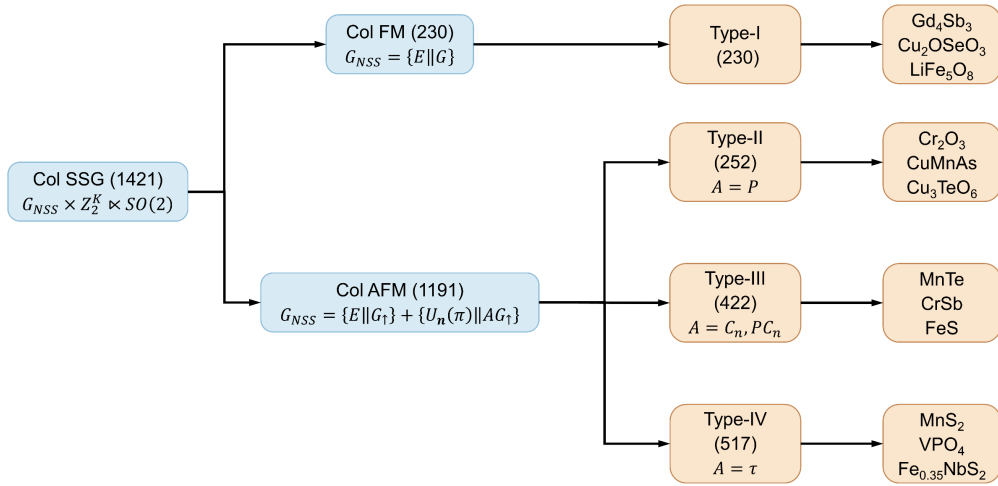


Fig. 1 | Classification of 1421 collinear SSGs for collinear magnets. For collinear FM, the spin space group $G_{NSS} = \{E||G\}$ can be constructed from the space group G . For collinear AFM, the sublattice space group G_{\uparrow} , the space group G of magnetic cell and the space operation A that connects different magnetic sublattices are necessary for constructing $G_{NSS} = \{E||G_{\uparrow}\} + \{U_n(\pi)||AG_{\uparrow}\}$. The last column lists the material candidates for each category. Col: collinear; G_{NSS} : nontrivial SSG; τ : fractional lattice translation; P : spatial inversion; C_n : spatial rotations.

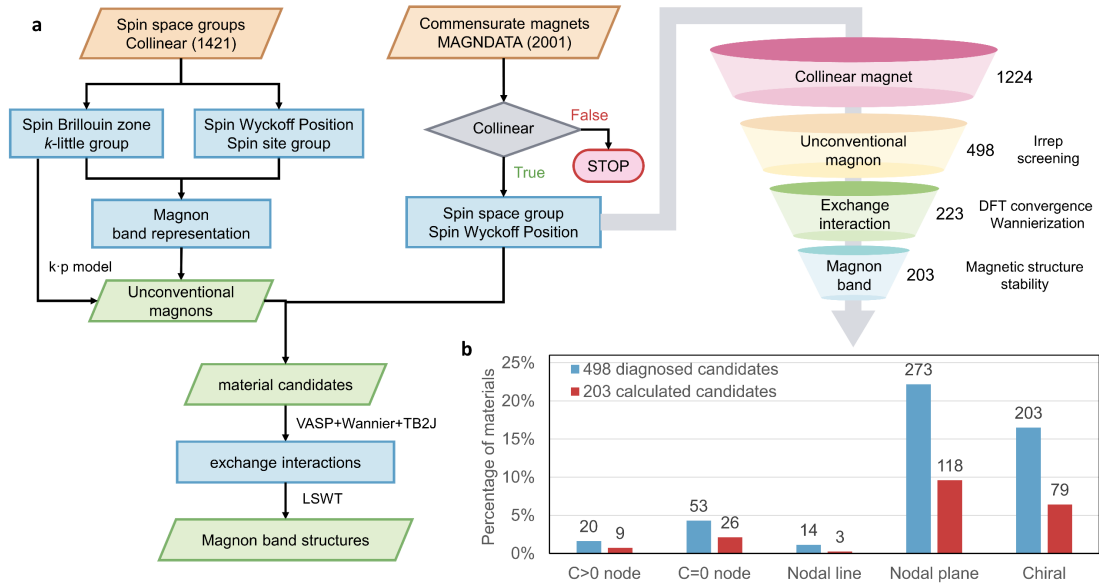


Fig. 2 | Workflow of the construction of the unconventional magnon database. a, First, 1224 collinear magnets are identified from the MAGNDATA database. Second, after the identification of the SSG, the irrep screenings are performed to obtain the material candidates hosting unconventional magnons. Third, the high-throughput calculations are performed to obtain all bilinear exchange interactions. Finally, unconventional magnon database with 203 magnon band structures and identified band representations are constructed. **b,** Statistics of different types of unconventional magnons in the collinear magnets from the MAGNDATA database.

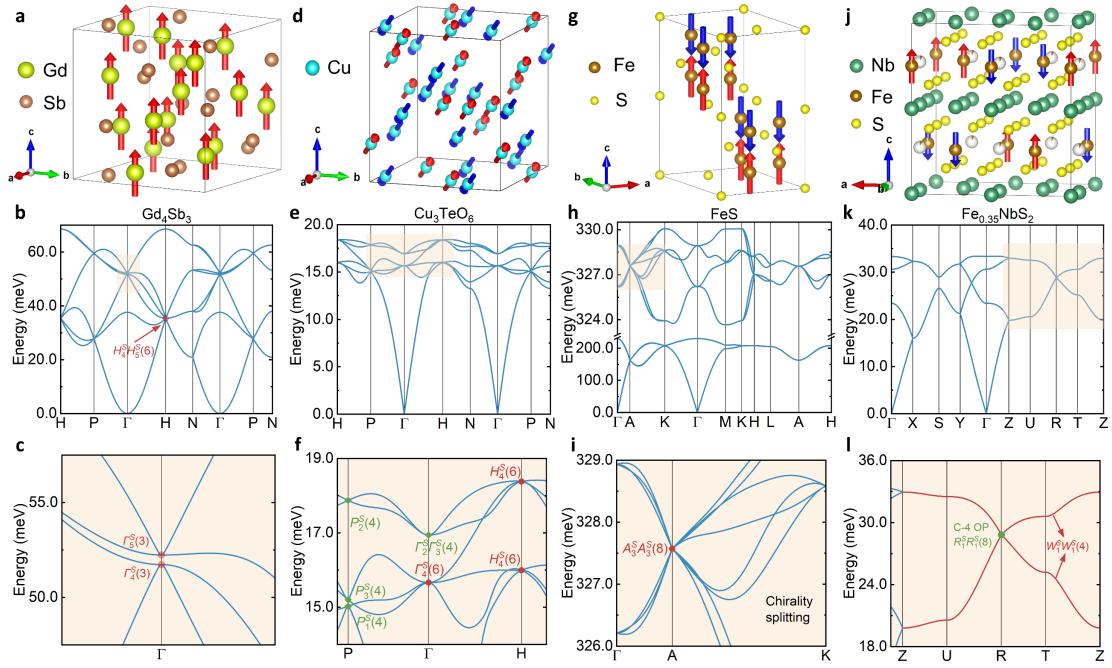


Fig. 3 | Four candidates hosting unconventional magnons. **a-c**, The collinear FM Gd_4Sb_3 , which has six-, four- and three-fold band crossings. **d-f**, The collinear AFM Cu_3TeO_6 with twelve-fold band crossing at R point. **g-i**, The altermagnet FeS , which has octuple degeneracy at A point and magnon chirality splitting along A-K line. **j-l**, The collinear AFM $\text{Fe}_{0.35}\text{NbS}_2$ with C-4 octuple magnons at R point, and red lines stand for the quadruple Z-U-R-T nodal plane. Schematic of Brillouin zone for each candidate can be found in Supplementary Information S7.